Computational study of gaseous cellular detonation diffraction and re-initiation by small obstacle induced perturbations

X.Q. Yuan,[1] C. Yan,[2] J. Zhou,[1] and H.D. Ng[2]
[1] *Science and Technology on Scramjet Laboratory, National University of Defense Technology, Changsha, 410073, China*
[2] *Department of Mechanical, Industrial and Aerospace Engineering, Concordia University, Montreal, Canada H3G 1M8*

(Dated: 5 April 2021)

Abstract

A gaseous detonation wave that emerges from a channel into an unconfined space is known as detonation diffraction. If the dimension of the channel exit is below some critical value, the incident detonation fails to re-initiate (i.e., transmit into a self-sustained detonation propagating) in the unconfined area. In a previous study, Xu *et al*. ["The role of cellular instability on the critical tube diameter problem for unstable gaseous detonations," Proc. Combust. Inst. **37**, 3545-3533 (2019)] experimentally demonstrated that, for an unstable detonable mixture (i.e., stoichiometric acetylene-oxygen), a small obstacle inserted in the unconfined space near the channel exit promotes the re-initiation capability for the cases with a sub-critical channel size. In the current study, numerical simulations based on the two-dimensional, reactive Euler equations were performed to reveal this obstacle-triggered re-initiation process in greater detail. Parametric studies were carried out to examine the influence of obstacle position on the re-initiation capability. The results show that a collision between a triple-point wave complex at the diffracting shock front and the obstacle is required for a successful re-initiation. If an obstacle is placed too close or too far away from the channel exit, the diffracting detonation cannot be re-initiated. Since shot-to-shot variation in the cellular wave structure of the incident detonation results in different triple-point trajectories in the unconfined space, for an obstacle at a fixed position, the occurrence of re-initiation is of a stochastic nature. The findings of this study highlight that flow instability generated by a local perturbation is effective in enhancing the re-initiation capability of a diffracting cellular detonation wave in an unstable mixture.

***Keywords**:* Detonation diffraction, cellular instabilities, obstacle-induced re-initiation, triple points

I. INTRODUCTION

When a propagating gaseous detonation wave emerges from a channel into an unconfined space, the diffracting detonation can either completely fail due to a continuous decoupling between the diverging shock and reaction zone (sub-critical case) or successfully re-establish a steady-state propagation in the unconfined space (super-critical case). The phenomenon of detonation diffraction has long been investigated since it provides a platform for investigating both propagation and initiation mechanisms of gaseous detonations.[1-4] The critical condition for successful transmission has been measured in many studies and generally characterized by the dimension of the channel exit scaled by λ, the intrinsic detonation cell size (e.g., for common unstable hydrocarbon mixtures, the critical channel diameter is given by $d_c = 13\lambda$)[5–10]. The recent experimental study by Nagura *et al.*[11] and later Kawasaki & Kasahara[12] also proposed a new length for scaling based on the reflection point distance (i.e., distance from the channel end corner to the reflection point of the transverse detonation on the channel end face). Using Vasil'iev's[13] smoked foils records, Lee[14] conjectured that, for common gaseous hydrocarbon mixtures, detonation failure is linked to the suppression of instabilities as a result of the diffraction. The successful transmission is invariably found to originate from localized explosion centers in the failure wave, where sufficient instabilities are maintained and eventually amplify to sustain the detonation propagation front in the open area.

Using high-speed schlieren photography[1,2] and advanced laser-based diagnostics[15], recent studies revealed more information on the detailed flow features during the diffraction of detonation waves. At the critical regime, successful transmission of a diffracting detonation wave requires a sufficient degree of cellular instability in the quasi-steady, weakly decoupled reaction-shock complex. The re-initiation mechanism is shown to be a consequence of local fluctuations at random locations within the region between the lead shock and decoupled reaction zone, resulting in the formation of an explosion bubble. In Fig. 1, for example, a sequence of high-speed schlieren photographs illustrates the key feature during the diffraction process of a Chapman-Jouguet C_2H_2 +2.5 O_2 detonation emerging from a 26.4-mm diameter tube at the critical condition of an initial pressure $p_o = 6.5$ kPa. Near the exit of the tube, a

decaying diverging shock wave is initially decoupled from the reaction front due to the influence of the expansion waves. Detonation cells grow in size as the number of transverse waves decreases. Nevertheless, some of the original transverse waves persist, subsequently creating a local explosion bubble. The bubble appears to grow near the tube axis where significant flow instabilities (i.e., cellular wave features) can still be observed near the diffracting wave front. Thus, this "surviving" cellular structure, i.e., the interaction among transverse waves within a quasi-steady shock-reaction wave complex, appears to be the dominant factor for the formation of the explosion bubble. A new transverse detonation is then formed and sweeps through the shocked but unreacted gas mixture toward the wall.

The importance of cellular instabilities in the outcome of the detonation diffraction has been further elucidated by Mehrjoo *et al.*[16,17]. Their studies show that, by generating artificially flow perturbations using small obstacles or by damping transverse waves using porous media at the tube exit, the transmission of a diffracting detonation wave can be promoted or suppressed, respectively. In the seminal work by Vasil'ev[13], re-initiation of a subcritical diffraction wave could be promoted via its reflection on a localized obstacle near the expanding cone in the open area. Following the same line of work, Xu *et al.*[1,2] in their experiments inserted a relatively smaller obstacle to promote the generation of transverse waves and to demonstrate the importance of the cellular instabilities at the diffracting front on the re-initiation, see Fig. 2. The use of this small obstacle can also act as a probe to identify the flow region where an explosion bubble can possibly form.

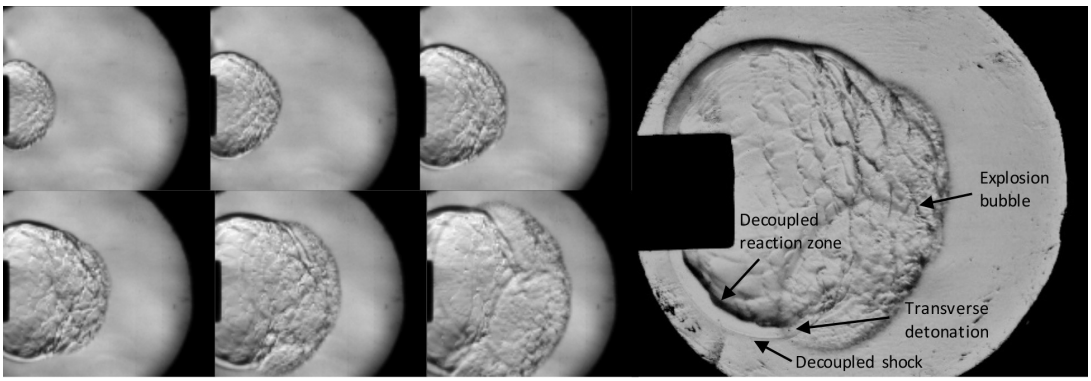

FIG. 1. The diffraction process and formation of the explosion bubble at the critical condition with $p_o = 6.5$ kPa. Note that these photographs were obtained from the experiments reported by Xu *et al.*[1,2].

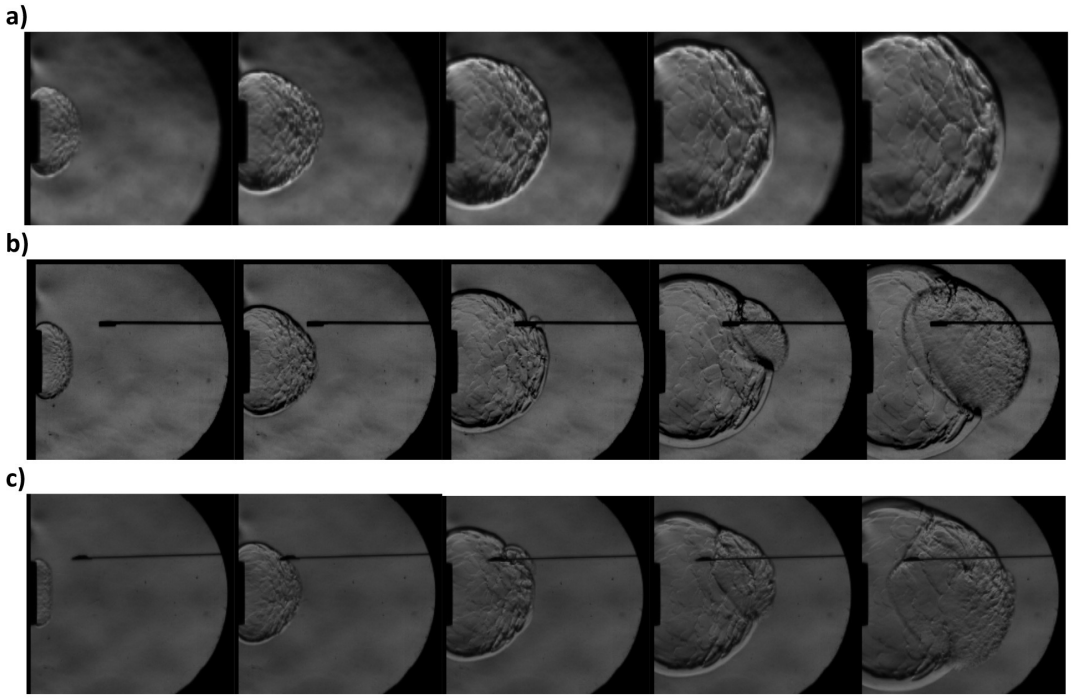

FIG. 2. Schlieren images showing a) the subcritical case of transition with $p_o = 5.7$ kPa and the effect of perturbation with b) $p_o = 5.0$ kPa at 36.5 mm; and c) $p_o = 3.8$ kPa at 26.5 mm. Note that these photographs were obtained from the experiments reported by Xu *et al.*[1,2].

The detonation diffraction problem has also been studied theoretically[18] and numerically, e.g.,[19–24]. Several numerical studies mostly attempt to reproduce the experimental scaling for critical conditions and perform parametric studies to reveal in detail different types of detonation diffraction: super-, sub-, and near-critical detonation diffraction. Notably, the numerical study by Jones *et al.*[25] also demonstrated the role of cellular instabilities on the $H_2/O_2/Ar$ detonation diffraction. Without any cellular structure, the diffracting wave failed when transmitted into a large volume. The presence of transverse waves in a cellular detonation leads to re-initiation of the detonation in an open area. This conclusion is further supported by the recent study of Shi *et al.*[22]. Their results show that the critical channel size for a successful transmission is smaller for a cellular detonation wave than that for a planar detonation wave. The effective collisions of transverse waves facilitate the re-initiation of a diffracting detonation wave via generating multiple randomly distributed hot spots.

In this work, numerical simulations are performed to further investigate the role of cellular

instabilities and re-initiation mechanism during the diffraction of detonation waves. In order to introduce perturbations, a small obstacle (of the order of a detonation cell size) is inserted in an open area into which an incident detonation wave transmits. The objective is to gain further insights into the promoting effect of obstacle-induced perturbations on the re-initiation of a diffracting detonation wave, complementing the experimental findings of Xu *et al.*[1,2]. The paper is organized as follows: In § 2, the ideal detonation model by the two-dimensional, reactive Euler equations with a two-step induction-reaction kinetic model[26,27]. The numerical methodologies for solving the governing equations are described. In § 3, simulation results are presented and the locations of the small obstacle where the induced effects can cause the re-initiation of the diffracting detonation wave are determined. The mechanism of the promoting effect by the obstacle in the re-initiation process and the implication of these results on the prominent role of cellular instabilities in detonation diffraction are then discussed. The influence of shot-to-shot variation in cellular dynamics is also illustrated. § 4 concludes the paper.

II. NUMERICAL MODEL DESCRIPTION

A. Governing equations

Neglecting diffusive processes, the governing equations for the detonation flow dynamics are simplified to the reactive Euler equations[28–30]:

$$\frac{\partial \mathbf{U}}{\partial t}+\frac{\partial \mathbf{F}}{\partial x}+\frac{\partial \mathbf{G}}{\partial y}=\mathbf{S} \tag{1}$$

$$\mathbf{U}=\begin{bmatrix}\rho\\ \rho u\\ \rho v\\ \rho e\\ \rho\xi\\ \rho\beta\end{bmatrix},\mathbf{E}=\begin{bmatrix}\rho u\\ \rho u^2+p\\ \rho uv\\ \rho u(e+p)\\ \rho u\xi\\ \rho u\beta\end{bmatrix},\mathbf{F}=\begin{bmatrix}\rho v\\ \rho uv\\ \rho v^2+p\\ \rho v(e+p)\\ \rho v\xi\\ \rho v\beta\end{bmatrix},\mathbf{S}=\begin{bmatrix}0\\ 0\\ 0\\ 0\\ \dot{\omega}_{\mathrm{I}}\\ \dot{\omega}_R\end{bmatrix} \tag{2}$$

with

$$e=\frac{p}{(\gamma-1)\rho}+\frac{1}{2}(u^2+v^2)-\beta Q \tag{3}$$

$$p=\rho T \tag{4}$$

The variables ρ, u, v, p, T, e, Q, denotes the density, velocities in x- and y-direction, pressure, temperature, energy and the amount of chemical heat release, respectively. The source terms are described by a two-step induction-reaction kinetic model[26,27] which was used in several previous studies, e.g.,[31–39].

$$\dot{\omega}_{\mathrm{I}} = \mathrm{H}(1-\xi)\rho k_{\mathrm{I}} \exp\left[E_{\mathrm{I}}\left(\frac{1}{T_{\mathrm{s}}}-\frac{1}{T}\right)\right] \tag{5}$$

$$\dot{\omega}_{\mathrm{R}} = [1-\mathrm{H}(1-\xi)]\rho(1-\beta) k_{\mathrm{R}} \exp\left[\left(-\frac{E_{\mathrm{R}}}{T}\right)\right] \tag{6}$$

where β is the product fraction, E_{R} is the activation energy of the exothermic reaction, E_{I} is the activation energy of the thermally neutral induction process, $\dot{\omega}_{\mathrm{I}}$ and $\dot{\omega}_{\mathrm{R}}$ are the chemical reaction rate during induction and reaction process and the Heaviside step function $\mathrm{H}(1-\xi)$ is given by:

$$\mathrm{H}(1-\xi) = \begin{cases} 1, & \xi \le 1, \\ 0, & \xi > 1. \end{cases} \tag{7}$$

All the flow variables have been made dimensionless by reference to the uniform unburned state ahead of the detonation front.

$$\rho = \frac{\tilde{\rho}}{\tilde{\rho}_0}, p = \frac{\tilde{p}}{\tilde{p}_0}, T = \frac{\tilde{T}}{\tilde{T}_0}, u = \frac{\tilde{u}}{\sqrt{\tilde{R}\tilde{T}_0}}, v = \frac{\tilde{v}}{\sqrt{\tilde{R}\tilde{T}_0}}, Q = \frac{\tilde{Q}}{\tilde{R}\tilde{T}_0}, E_a = \frac{\tilde{E}_a}{\tilde{R}\tilde{T}_0}. \tag{8}$$

The pre-exponential factor k_{I} of the induction step is chosen to define the spatial reference scale, so the induction length is unit, i.e., $\Delta_{\mathrm{I}} = 1$. In this study, the dimensionless thermodynamic parameters of the combustible mixture are $Q = 21.365$, $\gamma = 1.32$, $E_{\mathrm{I}} = 5.414\ T_{\mathrm{s}}$, $E_{\mathrm{R}} = 1.0\ T_{\mathrm{s}}$, $k_{\mathrm{I}} = 1.0022$, $k_{\mathrm{R}} = 4.0$, $T_{\mathrm{s}}/T_{\mathrm{o}} = 5.0373$ and the Chapman-Jouguet (CJ) Mach number $M_{\mathrm{CJ}} = 5.0984$ (or CJ detonation velocity $D_{\mathrm{CJ}} = 5.858$). These properties approximately represent a stoichiometric hydrogen-oxygen mixture at 20 kPa and 300 K giving rise to an unstable detonation wave with an irregular cellular pattern. The detonation velocity and Mach number are obtained from the thermodynamic equilibrium conditions using software like the NASA chemical equilibrium package CEA[40]. Following the procedure outlined in Radulescu and Maxwell[41], the heat release Q is approximated from the detonation Mach number using the specific heat ratio at the von-Neumann state. The determination of the induction activation energy follows the standard procedure in the literature from the constant volume explosion calculation [26], and the other kinetic parameters are calibrated to fit approximately the ZND profiles obtained from the

CHEMKIN calculation[42] with detailed chemistry of the corresponding mixture condition.

The solutions to the governing equations are obtained numerically using a second-order MUSCL-Hancock scheme with an HLLC (Harten – Lax – van Leer – contact) Riemann solver[43], with a CFL (Courant – Friedrichs – Lewy) number of 0.90. To accelerate the simulation, the entire flow solver was implemented in the Nvidia CUDA programming language[44–46] exploring the use of parallel computing enabled by an Nvidia Tesla K40 graphics processing unit (GPU). In this work, the default resolution considered is 16 computational grid points per induction zone length Δ_I, i.e., $\Delta_I/dx = 16$.

B. Simulation setup and numerical methods

The computational domain is shown in Fig. 3. Applying a mirror condition along the upper boundary, only half of the diffraction flow field was simulated. The size of the domain was made sufficiently large so that the entire diffraction and re-initiation process could be captured. A rectangular obstacle with dimensionless sizes of 50 × 5 was initially placed in the open area. The horizontal and vertical distances of the obstacle position, d_h and d_v, from the upper right corner of the obstacle to the expansion corner were varied. A detonation was first initiated and allowed to propagate for thousands of characteristic reaction zone lengths to reach a fully established CJ cellular detonation in a straight channel with width w. The corresponding flow field data of the CJ cellular detonation were then used as the initial conditions and placed near the channel exit for the diffraction simulations. In some simulations, especially for those in the critical regime, the incident cellular detonation fields were initialized at different locations so that the instabilities of the cellular front emerging from the channel was varied from simulation to simulation. As described in the next section, in the critical regime, the difference in the cellular characteristics of the detonation exiting the confined channel can lead to a different outcome for the transmission.

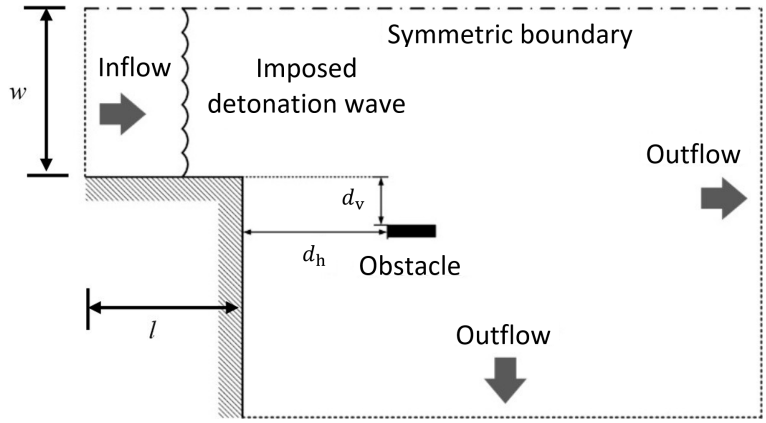

FIG. 3. Schematic of the computational domain

III. RESULTS AND DISCUSSION

A. A planar vs. cellular incident detonation wave

Following Shi *et al.*[22], numerical simulations were performed to illustrate the prominent role of cellular instabilities by comparing the critical conditions obtained using a planar ZND detonation and a cellular detonation imposed near the exit of the horizontal channel. Meanwhile, a study of numerical resolution was also performed to examine the effect of grid size on the resulting critical half channel width for successful re-initiation in the cellular detonation case.

As shown in Fig. 4, a finer grid tends to narrow the interval of the critical channel width. For each channel width in Fig. 4, simulations were repeated (as much as 10 times) with different initial cellular structures emerging from the channel. A circle symbol represents all these repeats at that channel width which result in re-initiation or described as the "*Go case*". A cross symbol represents all those repeats at that channel width which give failure or the "*No-Go case*". In the critical area, an overlapping of circle and cross symbols represents a mix of Go and No-Go cases depending on the initial condition. For the grid resolution with 5 computational grid points per induction zone length, $\Delta_I/dx = 5$, the critical regime lies between $w = 220$ and $w = 280$. For a higher grid resolution, i.e., $\Delta_I/dx = 16$, the critical range is reduced to around $w = 260 \sim 270$. By increasing the grid resolution, small-scale instabilities can be resolved. Increasing further the resolution will not significantly change the interval of critical condition. Hence, in this work, a resolution of $\Delta_I/dx = 16$ was used in this study as the default resolution.

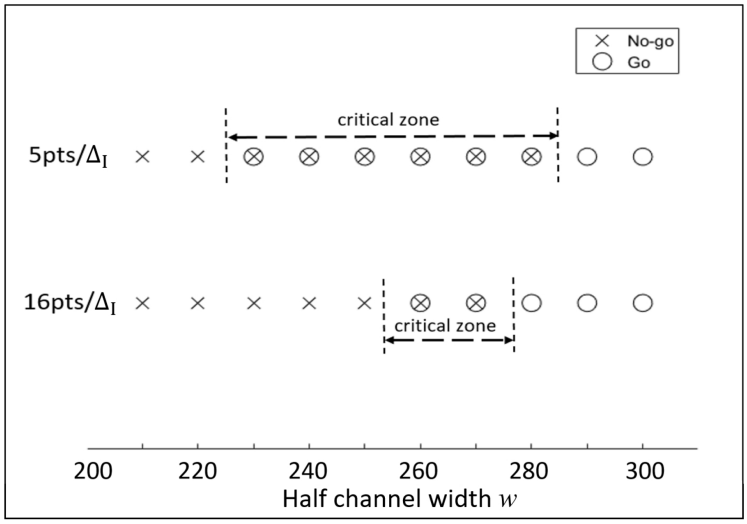

FIG. 4. Go and No-go cases for the grid resolution of $\Delta_I/dx = 5$ and $\Delta_I/dx = 16$

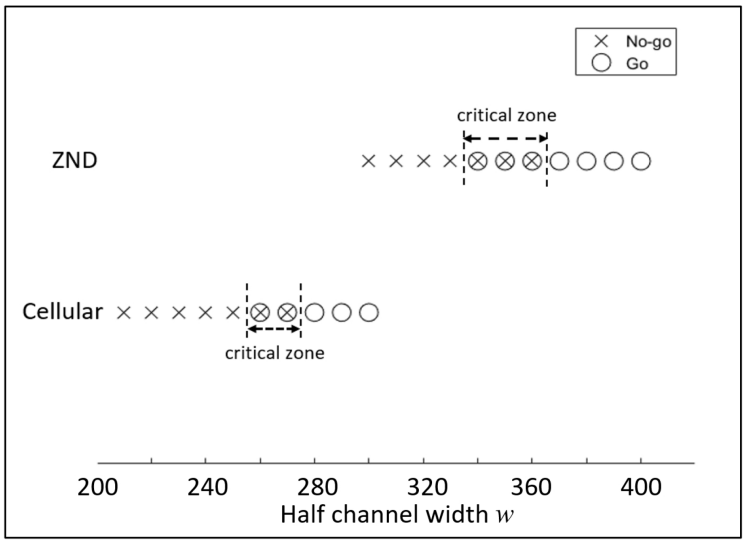

FIG. 5. Go and No-go cases for planar ZND detonation and cellular detonation

Figure 5 shows that the critical half channel width for planar ZND detonation diffraction lies between $w = 330 \sim 340$, while the critical value for cellular detonation diffraction is between $w = 260 \sim 270$. Hence, the critical half channel width resulted from a cellular detonation wave is smaller than that from a planar detonation wave. This distinct result in term of critical conditions thus indicates that the existence of cellular instabilities provides a possible promoting effect on the detonation transmission from the channel into the open area.

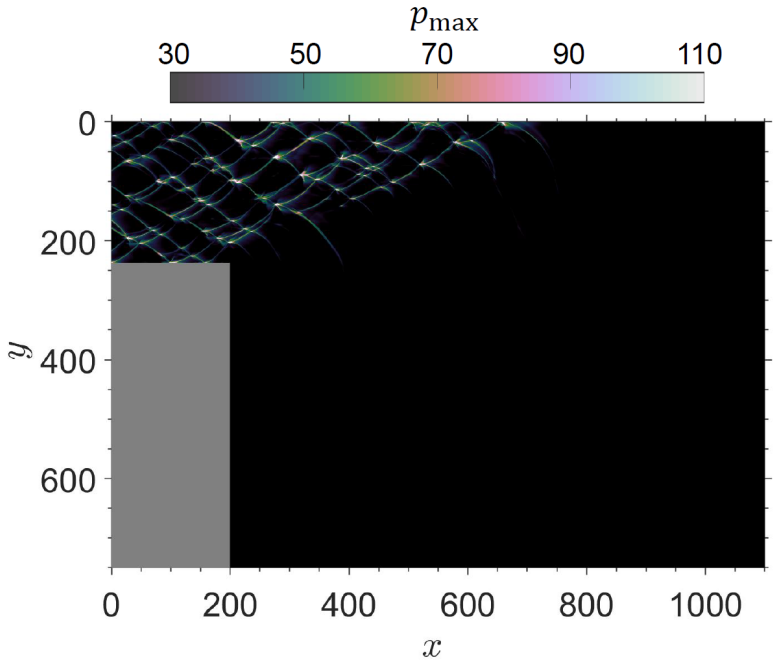

FIG. 6. Numerical soot foil for the detonation diffraction under the subcritical condition without an imposed obstacle at a half channel width w = 240.

B. A cellular incident detonation wave with an obstacle

For the subsequent simulations with the presence of an obstacle to induce instabilities, the computation was initialized by using the half-width w = 240 of the horizontal channel determined *a priori* in Fig. 5 to obtain a cellular detonation wave under the sub-critical condition. The cellular structure of the initial detonation wave, as well as the diffraction process without an obstacle, is presented by the numerical soot foil in Fig. 6. It can be seen that the cellular patterns vanish when the detonation wave propagates into the open area indicating a subcritical regime.

1. Obstacle-induced re-initiation process

The density and pressure contours in Fig. 7 show a typical re-initiation process induced by the rectangular obstacle in the open area. The obstacle position is d_h = 500 and d_v = 40. Since the diffraction regime is sub-critical without an obstacle, the central core of the wave front at the inner side can still sustain the detonation cellular structure when the detonation wave propagates into the open area, whereas the outer side part decouples immediately by the diffraction effect, and the cellular structure with transverse waves begin to vanish, as displayed in Fig. 7(a). When the decoupled, diverging wave

front reaches the edge of the imposed small obstacle, the oblique collision between the wave front and the obstacle induces an unsteady reflection structure on the surface of the obstacle, which enhances the pressure and temperature behind the reflected wave, as shown in Fig. 7(b). Although the increase in pressure and temperature due to the shock reflection from the obstacle ignites the unburned mixture in the decoupled region between the reaction zone and diverging leading shock, however it is still insufficient to generate a strong local explosion and the shock-reaction zone complex is still partially decoupled as demonstrated in Fig. 7(c). Immediately after the reflection, a detonation triple-point with a transverse wave sweeps down along the diffracting wave front, colliding with the reflection triple-point propagating upward. Figure 7(d) shows that this collision further increases the temperature behind the wave front again, leading to a local explosion and generating an explosion bubble. Originated from this explosion bubble, the combustion front, and the shock wave front are re-coupled upon forming a new transverse wave, indicating that a local detonation wave structure is formed. As this local detonation wave spreads out, the re-initiation occurs.

Figure 8 presents the corresponding numerical soot foil. A band of multiple cell structures can be seen (i.e., near the top-right corner of the soot foil), indicating a transverse detonation is formed and sweeping upward. Two bright regions, A and B, indicate the increase of pressure, which corresponds to the reflection of wave front on the obstacle surface and the collision between the triple points of detonation and reflection resulting into a strong explosion bubble, respectively. The simulation is also carried out in a much longer domain in x-direction to verify the re-initiated cells do not fade away or the detonation fails again. The detailed views shown in Figs. 7 and 8 suggest that the re-initiation process is driven by a sequence of mechanisms: An increase in pressure (and temperature) due to the shock-obstacle interaction results in a local increase in energy release rate behind the decoupled wave front; this more rapid energy release ignites the unburnt gas in the decoupled area and is the precursor to an explosion bubble generation leading to the re-initiation along the entire wave front.

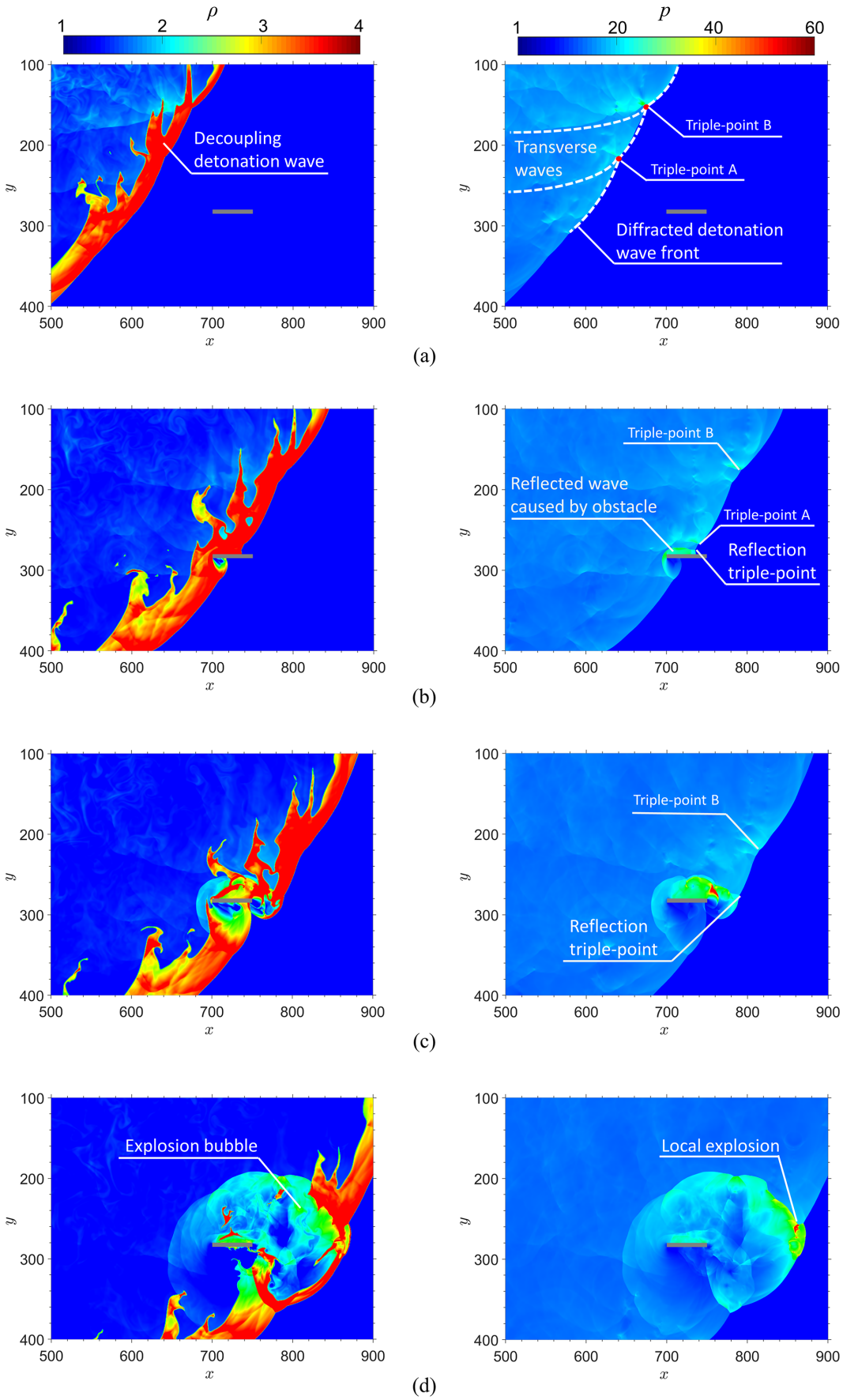

FIG. 7. Density (left) and pressure (right) contours presenting a successful re-initiation induced by an obstacle for (a) $t = 95$; (b) $t = 124$; (c) $t = 135$; and (d) $t = 151$

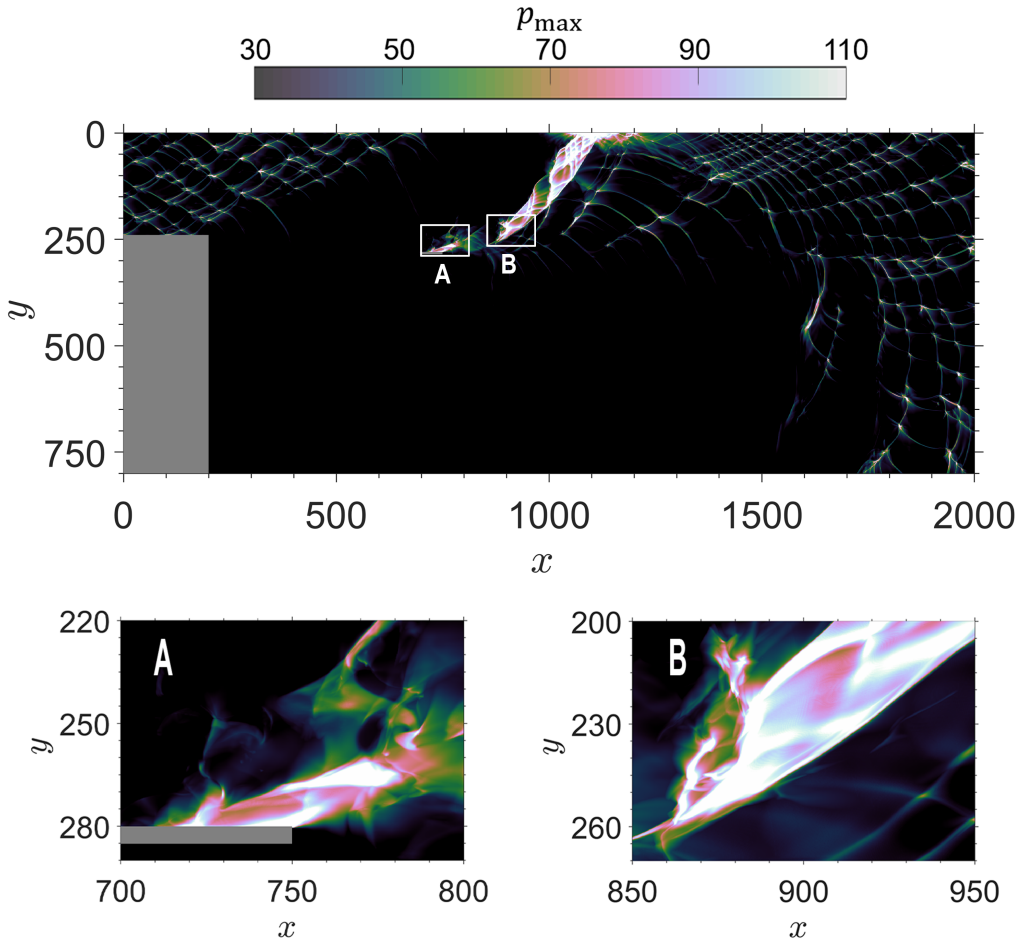

FIG. 8. Numerical soot foil for a successful re-initiation induced by an obstacle. (A) Reflection of wave front on the obstacle, (B) collision between the triple-points of detonation and reflection

2. Comparison between re-initiation and failure cases

The re-initiation or failure outcome due to obstacle-induced perturbations is further elucidated by some zoom-in views of the flow field (shown as contour plots of pressure) near the obstacle in Fig. 9. A failed re-initiation case, corresponding to an obstacle positioned at $d_h = 450$ and $d_v = 40$, is shown in Fig. 9(a). As a comparison, the same process for the successful case mentioned above is also presented, see Fig. 9(b). It can be found that a reflected triple-point wave structure is formed in both cases with an increase in pressure behind the reflected wave to approximately $p = 30$. The difference is that, in the successful case, there exists a triple point (associated with a transverse wave) from the incident diffracting detonation wave in close vicinity to the reflection area and traveling towards the obstacle. Subsequent collisions among the reflected triple point, the detonation triple point, and the obstacle surface hence take place within a very short period of time, which raises the pressure to $p \geq 60$ as

shown in Fig. 9(b). This sequence of significantly stronger wave-obstacle collisions more effectively induces a local explosion in the decoupled, unburnt region. While in the failed case, as shown in Fig 9(a), there is no immediate neighboring triple point from the incident diffracting cellular detonation (with a transverse wave propagating towards the obstacle), and the reflected shock pressure remains approximately p = 30 throughout the entire reflection process. Hence, although the triple points of detonation and reflection collide eventually afterward, the increase in local energy release rate upon such interaction is insufficient to cause re-initiation. This result also implies that the position and the number of transverse waves and triple points, or simply, the degree of cellular instabilities persisting in the incident diffracting detonation wave are important elements controlling the re-initiation capability of a diffracting detonation wave.

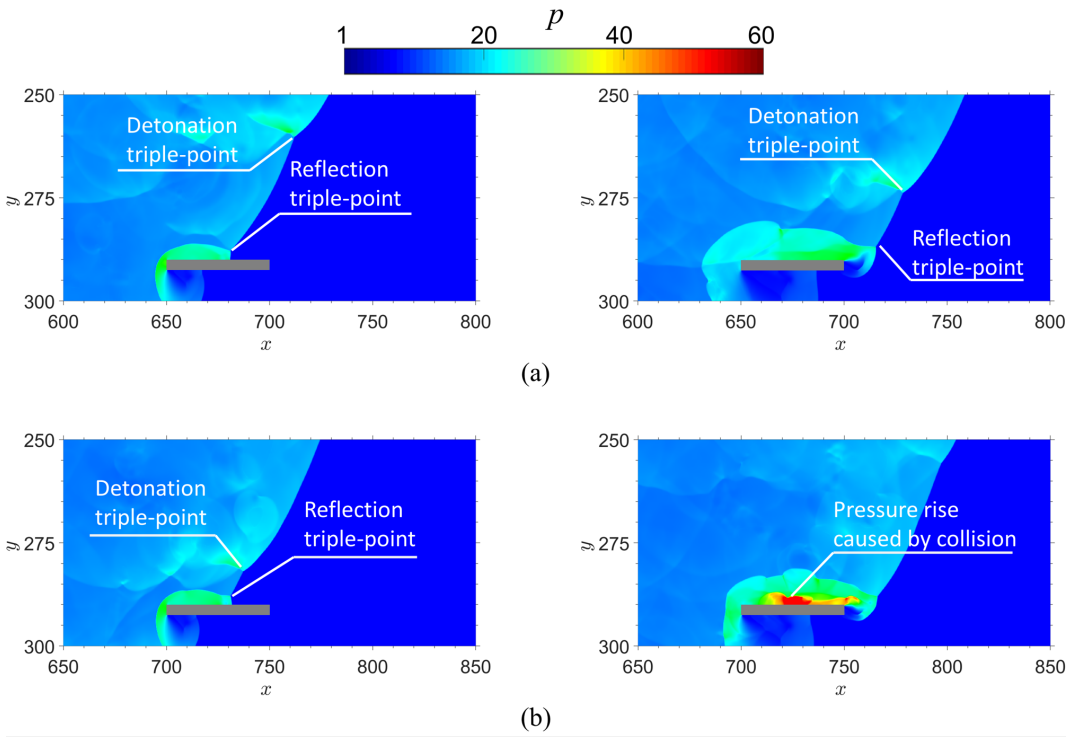

FIG. 9. Comparison of the reflection process between failed and successful cases. (a) Failed case with d_h = 450 and d_v = 40 at t = 112 (left) and t = 119 (right); and (b) Successful case with d_h = 500 and d_v = 40 at t = 123 (left) and t = 130 (right)

3. A parametric study on obstacle position causing re-initiation

To investigate the effect of the obstacle position on the re-initiation of the diffracting detonation wave, a series of simulations with the same initial and mixture conditions were conducted with various obstacle positions. The parameter d_h is varied from 50 to 700 with an increment of 50, and d_v is varied from −120 to 120 with an increment of 20. Recall that d_h and d_v are the horizontal and vertical distances of the obstacle from the corner of the channel exit (at $x = 200$ and $y = 240$ marked by the black circle in Fig. 10). The re-initiation result for each case is displayed schematically in Fig. 10, combined with the numerical soot foil with no obstacle. It can be observed that only a few obstacle positions result in a successful re-initiation. The successful cases distribute in an area of $100 \geq d_v \geq 40$ with obstacle positions intersecting or immediately neighboring the trajectories of detonation triple points (observed in Fig. 10 as the long bright traces stretched downward). The intersection indicates that a detonation triple point can reach the surface of the obstacle at a certain time, causing strong collisions and reflections, and significantly enhancing the energy release behind the reflected wave. As shown in Fig. 10, beyond a certain distance (in both x and y-direction) from the channel exit, even intersecting a triple-point trajectory, an obstacle cannot trigger re-initiation. This result thus indicates that there is also a minimum strength of a transverse wave along the diffracting shock front required for re-initiation. By examining the contour plots of p_{max} shown in Fig. 10, this minimum transverse shock (or triple-point) pressure is found to be approximately $p = 16$. In most cases with an obstacle not intersecting any detonation triple-point trajectory, re-initiation does not occur. This finding further demonstrates that a strong collision of a triple point along the diffracting shock front immediate with the reflected triple point from the obstacle is needed for re-initiation.

Inside the region ahead of the trajectory of the expansion wave front (approximately marked by the white dashed line in Fig. 10), the cellular detonation is not yet affected by the diffraction and any perturbation will not significantly influence its propagation. In addition, in the vicinity of the expansion wave front, the persisting transverse waves become weak and the detonation wave front is not completely decoupled from its reaction zone so that there is no sufficient unburnt gas in the decoupled

region to amplify the reflected wave and hence, ignite and induce a strong local explosion for detonation re-initiation. Thus, an obstacle that is placed too close to the central axis of the channel, i.e., $d_v < -40$, cannot induce re-initiation. Another possibility to promote the re-initiation is to vary the obstacle orientation to enhance the reflected transverse wave strength and its subsequent amplification which is however beyond the scope of this paper. In the area of $d_v > 100$, the diffracting shock wave is fully decoupled from the reaction front and has barely any transverse waves (or triple points) to cause strong collisions with the obstacle. For this reason, an obstacle that is placed too far from the channel exit also fails to re-initiate the detonation.

In all of the successful cases, the results from Fig. 10 also show that there is at least one long trajectory of detonation triple point downstream from (i.e., on the right side of) the obstacle to warrant the re-initiation. This appears to indicate that the explosion bubble resulting from the strong collision between a detonation triple point and the reflected wave from the obstacle needs to grow and be further enhanced or amplified by interacting with at least another triple point downstream inherent from the incident cellular detonation to give rise to a local explosion. As shown in Fig. 10, the obstacles placed along the downstreammost (i.e., rightmost) triple-point trajectory do not result in re-initiation.

To verify whether the above-described obstacle-induced re-initiation mechanisms are independent of any shot-to-shot variation in the cellular structure of the incident detonation wave, two series of simulations were performed with an initially different cellular detonation structure emerging from the channel (shown in Fig. 10(a) and (b)). Due to the difference in the cellular characteristics of the incident detonation, the obstacle locations for successful re-initiation differ in Fig. 10(a) and (b). These two sets of results, however, consistently indicate that only obstacles placed closely along the triple points trajectories of the incident diffracting cellular detonation can induce the re-initiation, and those intersecting with the trajectory of the downstreammost triple-point trajectory (i.e., no following triple points from the incident detonation persist) fail to cause re-initiation. This finding implies that, if an obstacle is placed at a fixed position (with respect to the laboratory reference frame), the occurrence

of re-initiation is of a stochastic nature depending on the intrinsic wave structure of the incident detonation wave.

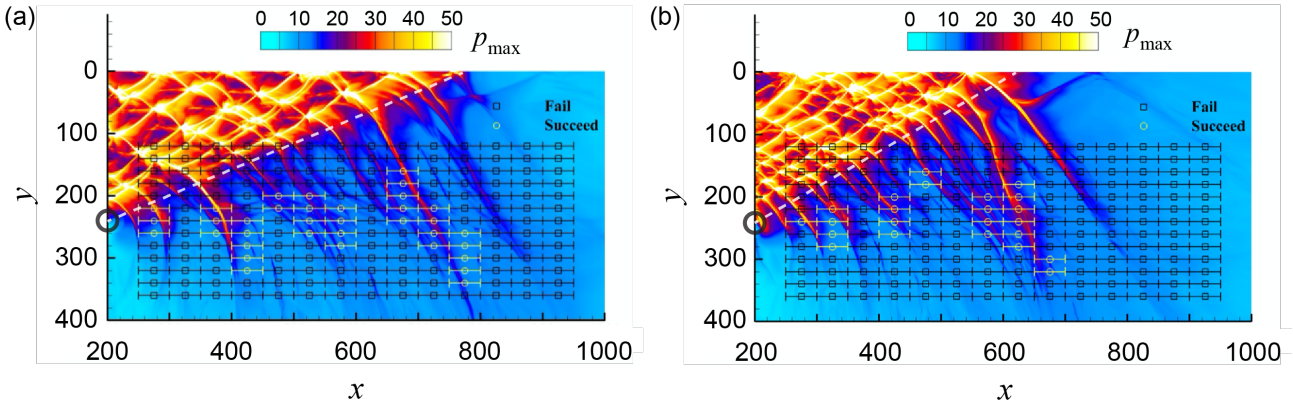

FIG. 10. The Go and No-go results for the cases with different obstacle positions marked the symbols with a horizontal bar mapped on the corresponding numerical soot foil for the incident cellular detonation wave. White circles indicate the cases of a successful re-initiation and black squares indicate the cases of failure. The corner of the channel exit is marked by the black circle on the y-axis. The trajectory of the expansion wave front is marked by the white dashed line. For the same channel width $w = 240$, the results of two series of simulations with different incident cellular detonation structures are shown in (a) and (b).

IV. CONCLUDING REMARKS

In summary, this work investigates numerically the effect of small obstacle-induced perturbations on the re-initiation of a diffracting detonation wave in an unstable mixture of detonable gases. The computational model in this numerical investigation is based on the reactive Euler equations, which is simpler and of lower accuracy than Navier-Stokes or discrete kinetic models, such as the method of Lin *et al.*[47, 48]. The conclusions are reliable enough based on the current Euler equations, although the latter methods could provide more accurate predictions. The simulation results demonstrate that an incident detonation wave with fully developed cellular instabilities is prone to re-initiation in the unconfined space than a planar (laminar-like ZND) incident detonation. In agreement with the experimental findings of Xu *et al.*[1,2], the current results show that a small obstacle inserted at certain locations relative to the diffracting detonation wave promotes the propensity of re-initiation. These results support the hypothesis that, for a successful re-initiation in an unstable mixture, a sufficient

degree of flow instabilities (either survived naturally from the incident detonation or induced artificially by a small obstacle) is required to induce an explosion bubble for the onset of re-initiation. The parametric study reveals that an immediate collision between a diffracting triple-point wave and the reflected wave from the obstacle is a necessary condition for generating a strong explosion bubble for a successful re-initiation. Subsequent interaction and amplification of the explosion bubble by the few remaining triple points along the diffracting cellular detonation also warrants the detonation re-initiation. Due to shot-to-shot variation in the trajectories of diffracting triple points, the re-initiation capability for a fixed obstacle position is of a stochastic nature.

Although a direct quantitative comparison with the experimental results of Xu *et al.*[1,2] is not feasible primarily due to the three-dimensional effects in the experiment and the complex reaction kinetics of the real combustible mixture, the present numerical study should still provide some insights on the salient flow features from the local shock-obstacle interaction and key mechanism leading to the detonation re-initiation. This numerical study once again highlights qualitatively the importance of cellular instabilities and the fact that for the cellular detonation diffraction, there should be sufficient local triple points (or cells) to amplify another local disturbance and form the re-initiation bubble.

ACKNOWLEDGMENTS

This work is supported by the Natural Sciences and Engineering Research Council of Canada NSERC (No. RGPIN2017-06698) and the Key Laboratories Program of China (No. 6142704200101). The authors thank Xiaocheng Mi for comments and feedback on the manuscript.

DATA AVAILABILITY STATEMENTS

The data that support the findings of this study are available from the corresponding author upon reasonable request.

REFERENCES

[1] H. Xu, X. C. Mi, C. B. Kiyanda, H. D. Ng, J. H. S. Lee, and C. Yao, "The role of cellular instability on the critical tube diameter problem for unstable gaseous detonations," Proc. Combust. Inst. 37 (3), 3545–3553 (2019).

[2] H. Xu, X. C. Mi, J. Lee, X. Yuan, and H. D. Ng, "Diffraction and re-initiation of unstable detonations emerging from a confined tube to an open area," in *Proceeding of the Canadian Section of the Combustion Institute Spring Technical Meeting* (Ryerson University, Toronto, ON, Canada, 2018).

[3] D. H. Edwards, G. O. Thomas, and M. A. Nettleton, "The diffraction of a planar detonation wave at an abrupt area change," J. Fluid Mech. 95, 79–96 (1979).

[4] J. H. S. Lee, *Detonation Phenomenon* (Cambridge University Press, New York, 2008).

[5] V. V. Mitrofanov and R. I. Soloukhin, "The diffraction of multi-front detonation waves," Soviet Physics-Doklady 9 (12), 1055–1058 (1965).

[6] R. Knystautas, J. H. S. Lee, and C. Guirao, "The critical tube diameter for detonation failure in hydrocarbon-air mixtures," Combust. Flame 48, 63–83 (1982).

[7] H. Matsui and J. H. S. Lee, "On the measure of the relative detonation hazards of gaseous fuel-oxygen and air mixtures," Proc. Combust. Inst. 17, 1269–1280 (1978).

[8] I. Sochet, T. Lamy, J. Brossard, C. Vaglio, and R. Cayzac, "Critical tube diameter for detonation transmission and critical initiation energy of spherical detonation," Shock Waves 9, 113–123 (1999).

[9] B. Zhang, H. D. Ng, and J. H. S. Lee, "The critical tube diameter and critical energy for direct initiation of detonation in C_2H_2/N_2O/Ar mixtures," Combust. Flame 159 (9), 2944–2953 (2012).

[10] B. Zhang, H. D. Ng, and J. H. S. Lee, "Measurement and relationship between critical tube diameter and critical energy for direct blast initiation of gaseous detonations," J. Loss Prevention Proc. Ind. 26, 1293–1299 (2013).

[11] Y. Nagura, J. Kasahara, Y. Sugiyama, and A. Matsuo, "Comprehensive visualization of detonation-diffraction structures and sizes in unstable and stable mixtures," Proc. Combust. Inst. 34, 1949–1956 (2013).

[12] A. Kawasaki and J. Kasahara, "A novel characteristic length of detonation relevant to supercritical diffraction," Shock Waves 30, 1–12 (2020).

[13] A. A. Vasil'ev, "Dynamic parameters of detonation," in *Shock Waves Science and Technology Library, Vol 6: Detonation Dynamics*, edited by F. Zhang (Springer-Verlag, Berlin Heidelberg, 2012) Chap. 4.

[14] J. H. S. Lee, "On the critical tube diameter," in *Dynamics of Exothermicity*, edited by J. Bowen (Gordon and Breach, Amsterdam, 1996) Chap. 4, p. 321.

[15] F. Pintgen and J. E. Shepherd, "Detonation diffraction in gases," Combust. Flame 156 (3), 665–677 (2009).

[16] N. Mehrjoo, B. Zhang, R. Portaro, H. D. Ng, and J. H. S. Lee, "Response of critical tube diameter phenomenon to small perturbations for gaseous detonations," Shock Waves 24 (2), 219–229 (2014).

[17] N. Mehrjoo, Y. Gao, C. B. Kiyanda, H. D. Ng, and J. H. S. Lee, "Effects of porous walled tubes on detonation transmission into unconfined space," Proc. Combust. Inst. 35 (2), 1981–1987 (2015).

[18] B. L. Wescott, D. S. Stewart, and J. B. Bdzil, "On self-similarity of detonation diffraction," Phys. Fluids 16, 373–384 (2004).

[19] C. P. Li and K. Kailasanath, "Detonation transmission and transition in channels of different sizes," Proc. Combust. Inst. 28, 603–609 (2000).

[20] M. Arienti and J. E. Shepherd, "A numerical study of detonation diffraction," J. Fluid Mech. 529, 117–146 (2005).

[21] J. Li, J. Ning, C. B. Kiyanda, and H. D. Ng, "Numerical simulation of cellular detonations diffraction in stable gaseous mixtures," Propul. Power Res. 5 (3), 177–183 (2016).

[22] L. Shi, K. C. K. Uy, and C. Y. Wen, "The re-initiation mechanism of detonation diffraction in a weakly unstable gaseous mixture," J. Fluid Mech. 895, A24, 1–36 (2020).

[23] S. Gallier, F. Le-Palud, F. Pintgen, R. Mével, and J. E. Shepherd, "Detonation wave diffraction in H_2−O_2−Ar mixtures," Proc. Combust. Inst. 36, 2781–2789 (2017).

[24] X. Q. Yuan, X. C. Mi, H. D. Ng, and J. Zhou, "A model for the trajectory of the transverse detonation resulting from re-initiation of a diffracted detonation," Shock Waves 30, 1–15 (2019).

[25] D. Jones, G. Kemister, E. Oran, and M. Sichel, "The influence of cellular structure on detonation transmission," Shock Waves 6, 119–129 (1996).

[26] H. D. Ng and F. Zhang, "Detonation instability," in *Shock Waves Science and Technology Library, Vol 6: Detonation Dynamics*, edited by F. Zhang (Springer-Verlag, Berlin Heidelberg, 2012) Chap. 3.

[27] H. D. Ng, M. I. Radulescu, A. J. Higgins, N. Nikiforakis, and J. H. S. Lee, "Numerical investigation of the instability for one-dimensional Chapman-Jouguet detonations with chain-branching kinetics," Combust. Theory Modell. 9, 385–401 (2005).

[28] M. Reynaud, F. Virot, and A. Chinnayya, "A computational study of the interaction of gaseous

detonations with a compressible layer," Phys. Fluids 29, 056101 (2017).

[29] W. Han, Y. Gao, C. Wang, and C. K. Law, "Coupled pulsating and cellular structure in the propagation of globally planar detonations in free space," Phys. Fluids 27, 106101 (2015).

[30] Y. Liu, W. Zhou, Y. Yang, Z. Liu, and J. Wang, "Numerical study on the instabilities in H_2−air rotating detonation engines," Phys. Fluids 30, 046106 (2018).

[31] H. Teng, L. Zhou, P. F. Yang, and Z. L. Jiang, "Numerical investigation of wavelet features in rotating detonations with a two-step induction-reaction model," Int. J. Hydrogen Energy 45, 4991–5001 (2020).

[32] K. Wang, Z. Zhang, P. Yang, and H. Teng, "Numerical investigation of wavelet features in rotating detonations with a two-step induction-reaction model," Phys. Fluids 32, 046101 (2020).

[33] P. F. Yang, H. H. Teng, Z. L. Jiang, and H. D. Ng, "Effects of inflow Mach number on oblique detonation initiation with a two-step induction-reaction kinetic model," Combust. Flame 193, 246–256 (2018).

[34] K. C. Tang-Yuk, X. C. Mi, J. H. S. Lee, and H. D. Ng, "Transmission of a detonation across a density interface," Shock Waves 28, 967—-979 (2018).

[35] J. Li and J. Ning, "Experimental and numerical studies on detonation reflections over cylindrical convex surface," Combust. Flame 198, 130–145 (2018).

[36] J. Li and J. H. S. Lee, "Numerical simulation of Mach reflection of cellular detonations," Shock Waves 26 (5), 673–682 (2016).

[37] G. X. Xiang, X. Gao, W. J. Tang, X. Z. Jie, and X. Huang, "Numerical study on transition structures of oblique detonations with expansion wave from finite-length cowl," Phys. Fluids 32, 056108 (2020).

[38] X. Q. Yuan, J. Zhou, X. C. Mi, and H. D. Ng, "Numerical study of cellular detonation wave reflection over a cylindrical concave wedge," Combust. Flame 202, 179–194 (2019).

[39] C. Yan, H. H. Teng, X. C. Mi, and H. D. Ng, "The effect of chemical reactivity on the formation of gaseous oblique detonation waves." Aerospace (MDPI) 6, 62 (2019).

[40] S. Gordon, and B. J. McBride, "Computer program for calculation of complex chemical equilibrium compositions and applications," Tech Rep. 1311. NASA Reference Publication, 1994.

[41] M. I. Radulescu, and B. McN Maxwell, "The mechanism of detonation attenuation by a porous medium and its subsequent re-initiation," J. Fluid Mech. 667, 96–134 (2011).

[42] R. Kee, F. Rupley, and J. Miller, "CHEMKIN-II: A Fortran chemical kinetics package for the

analysis of gas-phase chemical kinetics," Document No. SAND-89-8009, 1989.

[43] E. F. Toro, *Riemann Solvers and Numerical Methods for Fluid Dynamics* (Springer-Verlag, Berlin, 2009).

[44] C. B. Kiyanda, G. H. Morgan, N. Nikiforakis, and H. D. Ng, "High resolution GPU-based flow simulation of the gaseous methane-oxygen detonation structure," J. Vis. 18 (2), 273–276 (2015).

[45] X. C. Mi, A. J. Higgins, H. D. Ng, C. B. Kiyanda, and N. Nikiforakis, "Propagation of gaseous detonation waves in a spatially inhomogeneous reactive medium," Phys. Rev. Fluids 2, 053201 (2017).

[46] X. C. Mi, A. J. Higgins, C. B. Kiyanda, H. D. Ng, and N. Nikiforakis, "Effect of spatial inhomogeneities on detonation propagation with yielding confinement," Shock Waves 28, 993–1009 (2018).

[47] C. Lin, and K.H. Luo, "Discrete Boltzmann modeling of unsteady reactive flows with nonequilibrium effects," Phys. Rev. E 99 (1), 012142 (2019).

[48] C. Lin, A. Xu, G. Zhang and Y. Li, "Polar Coordinate Lattice Boltzmann Kinetic Modeling of Detonation Phenomena," Commun. Theor. Phys. 62, 737–748 (2014).